Journal Pre-proof

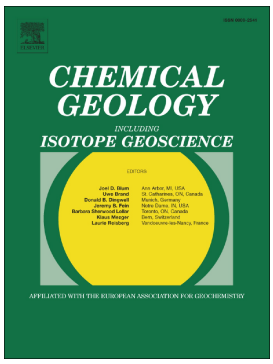

Volatility of mercury and related volatile metals at magmatic temperatures

Julien Boulliung, Bernard J. Wood, Tamsin A. Mather

PII: S0009-2541(25)00408-5

DOI: https://doi.org/10.1016/j.chemgeo.2025.123018

Reference: CHEMGE 123018

To appear in: *Chemical Geology*

Received date: 12 March 2025

Revised date: 22 August 2025

Accepted date: 23 August 2025

Please cite this article as: J. Boulliung, B.J. Wood and T.A. Mather, Volatility of mercury and related volatile metals at magmatic temperatures, *Chemical Geology* (2024), https://doi.org/10.1016/j.chemgeo.2025.123018

Volatility of mercury and related volatile metals at magmatic temperatures

Julien Boulliung[1,2], Bernard J. Wood[1*], Tamsin A. Mather[1]
[1]Department of Earth Sciences
South Parks Road
Oxford OX1 3AN
U.K.

[2]Centre de Recherches Pétrographiques et Géochimiques
15 Rue Notre Dame des Pauvres,
54500 Vandœuvre-lès-Nancy,
France

*corresponding author : bernie.wood@earth.ox.ac.uk

Abstract

The volatilities of metals in igneous systems are important constraints in the contexts of magmatic degassing, ore deposition and the volatile budgets of the Earth and other planets. In order to develop a systematic understanding of such volatilities, we have made the first experimental measurements of the volatility of Hg from molten basalt at high temperatures and compared it directly with other volatile trace elements (i.e., Ag, As, Cd, Cr, Cs, Cu, Ga, Ge, In, Li, Pb, Rb, Sb, Sn, Tl and Zn). We placed 100 mg of crushed basalt, containing 93 ppm of Hg and ~500 ppm of most of the other volatile metals in an alumina crucible which was sealed under vacuum inside a silica glass tube of volume ~4.4×10^{-6} m^3. After holding them at high temperature (1250, 1300 or 1400 °C) between 5 minutes and 24 hours, samples were quenched in air. Analysis of the quenched glasses using a Direct Mercury Analyser shows that almost all Hg (>99 %) is lost within the first few minutes, establishing a total pressure of Hg species of 150 Pa (calculated from the known mass of Hg in the system and the ampoule volume). Apparent steady-state concentrations of ~40 ppb Hg at 1400 °C and ~100 ppb Hg at 1300 °C are achieved after 1 and 6 hours respectively. The oxidation state of Fe in the products, measured by XANES, indicates that $Fe^{3+}/(Fe^{3+}+Fe^{2+})$ remains constant at ~0.1 during the experiments. The behavior of elements other than Hg in the glasses were determined by Electron Microprobe and Laser Ablation ICP-MS. In our experiments we find that the fraction of each element lost to the atmosphere decreases in the following order: Hg>>Tl>Cd>In>Zn*>Li>Cs>Cu*>As>Ag>Pb~Sn~Ga>Ge~Sb (with the position of asterisked elements uncertain and maximum possible volatilities adopted). These results show broad similarities to, but also important differences from volatilities estimated from field measurements of gas/aerosol compared to concentrations in lava. They also show important differences from volatilities obtained from open-system experiments and those

estimated from the condensation temperatures of elements in the relatively reduced environment of a protoplanetary gas disc.

Keywords: mercury volatility from silicate melt; trace metal volatility from melts; volcanic degassing of volatiles; volatility from basaltic melts.

1. Introduction

Determining the volatilities of trace metals from silicate melts is important for understanding their release to the atmosphere in volcanic systems (Mather, 2015) and to provide insights into their use as tracers of igneous/magmatic processes and wider processes associated with the composition, evolution and differentiation of silicate planets (e.g., Wood et al., 2006). An understanding of metal release from magmas also aids our understanding of the formation of some ore deposits (e.g., Blundy et al., 2021; Pokrovski et al., 2013; Williams-Jones and Heinrich, 2005). In the context of porphyry copper (Cu) deposits for example, Cu enrichment is mostly related to hydrous fluids exsolved from evolved magmas during magma ascent or crystallization (e.g., Hedenquist and Lowenstern, 1994; Cooke et al., 2014). In an enviromental context, volcanic emissions are an important source of trace metals and for some (e.g., Hg and Cd) they contribute up to 50 % of naturally occurring present-day release to the environment (e.g., Hinkley et al., 1994; Nriagu, 1989). Understanding the release of these often toxic trace metals from volcanoes yields insights into their impacts on animal/plant health (e.g., Martin et al., 2009) and they are important signals in archives of volcanic activity and environmental impacts such as ice cores (e.g., Hinkley and Matsumoto, 2007; Kellerhals et al., 2010). More specifically, previous work on Hg has shown its great potential in global chemostratigraphy and its ability to shed light on the links between past episodes of large-scale volcanism, namely large igneous provinces (LIPs), and global

environmental change events such as mass extinctions and carbon cycle perturbations (e.g., Sanei et al., 2012; Percival et al., 2021).

Hg analysis of sedimentary rocks and the identification of concentration "spikes" in the rock record is an area of growing interest with the potential to identify increasingly detailed insights into extended periods of Earth's geological history (e.g., Fendley et al., 2024). However, there is a lack of understanding of the way in which trace metals and particularly Hg behave in, and degas from, silicate melts and about how the emissions of these elements are related to the volumes, compositions, temperatures, and pressures of erupted/intruded melts. Hg behavior is particularly poorly understood due to low concentrations in natural samples and measurement challenges (especially with *in situ* techniques; e.g., low ionization potential, its high number of naturally occurring isotopes and stickiness). For example, measurements of the Hg contents of a large number of igneous rocks made using a Direct Mercury Analyser (Marie et al., 2015) led to a maximum observed concentration in basalt of 46 ± 6 ppb (parts per billion) and in granite of 155 ± 2 ppb. Most igneous rocks contain <11 ppb of Hg (Marie et al., 2015). These relatively low Hg contents highlight the volatile behavior of Hg with this element partitioning preferentially into the gas phase. For these reasons, it is difficult to determine the original magmatic Hg content. Hg is also volatile during volcanic eruptions (Pyle and Mather, 2003), but it appears to be retained sufficiently well by silicate melts that its incompatibility in silicate minerals can lead to modest enrichments during igneous differentiation. The volatility of Hg in volcanic systems is readily compared with that of other metallic elements using a partition coefficient approach. Zelenski et al. (2021) calculated the Hg partition coefficient (*Kd*) ($K_d = C_{Hg}^{gas}/C_{Hg}^{melt}$) between volcanic gas and a silicate melt system for arc and rift/hotspot magmatic contexts. These authors found that Kd_{Hg} in arc magmatic systems is of the same order as Kd_{Cu} and Kd_{Ag}; ~ 25 times lower than Kd_{Cd} and 5 and 20 times higher than Kd_{Zn} and Kd_{Li} respectively. However,

Kd_{Hg} has high uncertainty (i.e., > half an order of magnitude), since Hg content measurements in gas and silicate melts for the same volcanic system are very sparse.

In addition to regional scale volcanic degassing, a better understanding of magmatic Hg behavior will aid a wider understanding of planetary geochemical evolution. Hg is an element of low abundance in the bulk silicate Earth with an estimated concentration of ~6 ppb (Palme and O'Neill, 2014). This represents depletion by a factor of 60 relative to its accepted concentration (350 ppb) in CI chondrite meteorites commonly used as a model for the refractory element concentrations in the bulk Earth. For comparison, corresponding depletions of some other volatile elements are by factors of 34 (Tl), 19 (Cd) 7 (Cu), and 6 (Zn) (Palme and O'Neill, 2014). These elements (and Hg) are generally assumed to be part of a "volatility trend" of increasing depletion in bulk silicate Earth with increasing volatility (McDonough and Sun, 1995). Volatility, in this context is normally defined in terms of the temperature at which 50 % of the element of interest would be condensed at equilibrium from a gas of solar composition at a total pressure of 10^{-4} bar (Lodders, 2003). In this case condensation temperatures of 240K (Hg), 365K (Tl), 502K (Cd) 704 K (Zn) and 1034K (Cu) (Wood et al., 2019) correlate reasonably well with the observed depletions but should not be taken as indicative that condensation to a solid at low temperatures is the primary process by which their concentrations in silicate Earth were established.

Finally, Hg methylation via microbial processes in aqueous environments leads to the formation of methylmercury (MeHg). This is a bioaccumulating Hg species which can cause severe neurological and physiological damage to complex organisms if ingested (Driscoll et al., 2013; Wang et al., 2019). The ecological and societal risks of environmental Hg contamination highlight the importance of quantifying and understanding natural as well as anthropogenic emissions. Volcanism is one of the principal mechanisms of Hg release to the

atmosphere, hydrosphere and biosphere and thus all efforts to improve our understanding of its emissions from magmas are important (Pyle and Mather, 2003). For this reason, and the others discussed above, Hg is the main focus of our study although we will make comparisons with other volatile metals in order to place our results in context.

The principal hypothesis underlying the present study is that erupting lavas lose essentially all of their Hg, with gaseous Hg^0 as the prevalent form, to the H_2O-CO_2 rich gases emitted prior to and during subaerial eruptions (e.g., Bagnato et al., 2007; Bagnato et al., 2014). Here our aim is to better understand Hg behavior in basaltic melt, and the capacity of a magma to retain Hg under relatively high Hg partial pressures. These data will be used to constrain Hg volatility in basalt at magmatic conditions and to compare this volatility with other elements known to be volatile at high temperatures such as Tl, Cd, Cu and Zn. By using a sealed ampoule at atmospheric pressure we are able to determine the partial pressure of Hg species in equilibrium with a melt containing a known concentration of Hg at high temperature. Equilibrium speciation calculations, discussed in more detail below, indicate that Hg should be present in the gas phase largely as uncomplexed Hg^0 in both our experiments and in nature which means that chemically our data are directly applicable to nature, irrespective of the exact major element composition of the emitted gas. Analysis of Hg in quenched melts is difficult because the concentrations are too low for electron microprobe analysis and Hg does not ionize readily in Inductively-Coupled Mass Spectrometry (ICP-MS). However, analysis using a Direct Mercury Analyser that combines thermal decomposition, catalytic conversion, amalgamation, and atomic absorption spectrophotometry (e.g., Roy and Bose, 2008) is precise and accurate at the ppb level provided sufficient material is available and the sample is heated to high enough temperature to liberate all the Hg. Our volatility experiments were aimed, therefore, at yielding measurable Hg concentrations in melts in equilibrium with Hg-bearing gas at ~1 bar. The results provide constraints on the proportions of Hg expected to be lost

from erupted melts, the quantities anticipated to be emitted from LIPs of known volume as well as more general insights into Hg volatility.

2. Material and Methods

2.1 Experiments

To study Hg behavior in basaltic melts, we first attempted experiments at 1 atm in a vertical atmospheric furnace using platinum wire (0.2 mm in diameter) to support 4-5 mg of starting material, here an Icelandic basalt composition from Reykjanes Ridge, well characterized in previous studies (i.e., Norris and Wood, 2017; Thomas and Wood, 2021; Boulliung and Wood, 2022, 2023). These experiments involved addition of ~1000 ppm of Hg, as HgO, to powdered natural Icelandic basalt in order to determine if the Hg would be retained by the melt during an initial period of heating to the liquidus followed by immediate quenching. As expected, the results indicated almost complete loss of HgO during the initial heating stage (i.e., the time taken for the starting material to reach the liquidus temperature). We therefore opted to work with closed systems in which the Hg-bearing melt is sealed and Hg-retained inside a closed silica-glass ampoule or SSAS (Sealed Silica Ampoule System). This approach has previously been used to study other volatile elements notably alkalis in silicate melts (Tsushiyama et al., 1981; Mathieu et al., 2008). Experimentally the sealed tube, when placed in a furnace at known temperature, enables assessment of the partial pressures of the elements of interest as well as, given relevant thermodynamic data, their activities in the silicate melts.

For the SSAS experiments, we doped the starting material with ~500 ppm of each of a large number of trace elements exhibiting a wide range of volatility behaviors (i.e., Ag, As, Cd, Cl, Co, Cr, Cs, Cu, F, Ga, Ge, In, Li, Mo, Ni, Pb, Rb, Sb, Sc, Sn, Sr, V, W, Y, Zn, Zr). The doped starting composition was fused in a covered alumina crucible at 1 atm/1300 °C for 5 minutes and drop-quenched into water. The procedure was repeated and the 2 glasses combined to form a single starting material. After crushing and grinding, 93 ± 3 ppm of Hg was added as HgO powder. This final composition reported in Table 1 was used in multiple SSAS experiments and Hg contents were measured 5 times to ensure homogeneity in the starting material.

The SSAS preparation consists of several steps. The starting material (~100 mg powder) was first placed in an alumina crucible (5-mm outer diameter with 3-mm inner diameter and 10-mm long). The crucible was inserted into a silica tube (10-mm outer diameter with 8-mm

inner diameter) sealed at one end. The silica tube was then connected to a vacuum line overnight to decrease the inner pressure to ~2.7 mbar. This step is essential to prevent overpressure (>> 1 bar) during high-temperature experiments, as the inner pressure increases with temperature. The other extremity of the tube was sealed while still evacuating, yielding an ~9 cm long ampoule ready for the experiments.

In order to check for Hg loss during ampoule evacuation and sealing we performed a blank test in which the sample was evacuated and sealed and then opened and analyzed for Hg. This blank test showed that no Hg is lost during ampoule preparation. In order to facilitate comparison between experiments of different temperature and time we maintained the volumes of the ampoules (4.4×10^{-6} m^3) and the amounts of starting material (100 mg) as constant as possible for each experiment.

Experiments were performed in a muffle furnace at three different temperatures (1250, 1300 and 1400 °C) and for durations from 5 minutes to 24 hours. A thermocouple was used to check temperature consistency in the furnace and that the temperature is constant over the length of the ampoule with variations estimated not to exceed ± 5 °C (Mathieu et al., 2008; Mathieu, 2009). The silica ampoule was quenched in air at the end of the experiment (Figure 1). Some pieces of the product glass were selected for Hg analysis and others were mounted in epoxy and polished for microanalysis. We also analyzed a few parts of the silica ampoules and the alumina crucibles to check for Hg deposition. Figure 1 shows an ampoule after quenching.

2.2 Analyses

2.2.1 Starting material

The powdered starting material composition (Table 1) was determined after crushing and grinding and addition of 93 ± 3 ppm of Hg. Major and trace elements were analyzed at the CNRS Service d'Analyse des Roches et des Minéraux (SARM; in Nancy, France). Major elements were analyzed by ICP-OES (iCAP 6500 Radial from Thermo Scientific®) and most trace elements were analyzed by flow injection ICP-MS (see details in Carigan et al., 2001). Li contents were determined by atomic absorption using the Flame Atomic Absorption Instrument 240FS from Agilent®, Cl by Na_2CO_3 alkali fusion followed by spectrophotometry (using Cary 60 UV-Vis Spectrophotometer from Agilent®; see details in Vernet et al., 1987) and F by potentiometric analysis using a fluoride-ion sensitive electrode from Metrhom® (e.g., Vernet et al., 1987; Foucaud et al., 2019).

Trace element contents of the starting materials were additionally checked by Laser Ablation ICP-MS on separate chips of glass from each of the 2 fusions using the methods

described below. As can be seen from Table 1, there is very good agreement between the 2 independent methods of analysis, at SARM, Nancy and in Oxford.

2.2.2 Product compositions

The major element compositions of the final glass run products (Supplementary Table S1) were determined using a CAMECA SX-Five-FE microprobe in the Department of Earth Sciences, University of Oxford. Analytical conditions were 15 kV accelerating voltage, 40 nA beam current with a spot size of 20 μm. The standards used for the calibration were natural albite (Si, Al, Na), wollastonite (Ca), fayalite (Fe), sanidine (K), TiO_2 (Ti), MgO (Mg), NaCl (Cl), BaF_2 (F), pyrite (S) and copper metal (Cu). Approximately 9 points were analyzed on each sample to check for homogeneity with, in addition, where possible, measurements of any compositional gradients from the alumina crucible edge to the center also determined (Supplementary Table S1).The same methods were used to determine F and Cl contents of the starting glasses with a total of 325 analyses made of 13 chips of starting glass (Table 1). The overlap of the Fe Lα line on the F background was corrected-for using the inbuilt Cameca software. An independent check of this method, with good agreement, was performed by calibrating the apparent negative F contents measured in Fe-bearing F-free materials (almandine, fayalite, St. Johns Island olivine).

As observed by Neuman et al. (2022) for longer experiments, spinel precipitation may occur at the contact between the alumina crucible and the melt. In order to determine if solids precipitated during our experiments, backscattered electron (BSE) images were collected by scanning electron microscope (SEM) JEOL JSM-6510 at the Centre de Recherches Pétrographique et Géochimiques (CRPG, Nancy, France). For the observations, we used a 3 nA beam current with accelerating voltage of 15 kV. Images and further information are reported in Supplementary material A.

The mercury content of each sample (Supplementary Table S2) was determined using DMA-80 evo from MILESTONE® (Direct Mercury Analyzer; e.g., Marie et al., 2015). The DMA-80 evo was calibrated using a range of standards (NIST glasses, basalts, sediments; Marie et al., 2015) re-analyzed during and after each series of samples. These standards contain different Hg contents ranging from 12±1 (BEN) to 1580 (110) ppb (see Marie et al., 2015 for more details). A minimum of two basaltic standards (with Hg contents of 12 ± 1 and 101 ± 10 ppb) were analyzed to avoid potential matrix effects. Blank measurements were also included in the analytical runs to check for memory effects especially after samples showing relatively high Hg concentrations. For example, after analysis of a sample containing 1755 ± 175 ppb Hg,

the blank level was 0.4 ± 0.4 ppb. Various blank measurements, depending on previous Hg content measurements, were analysed to ensure that the memory effect contribution is < 0.5 ppb. To determine Hg homogeneity in the melt and reproducibility of the analyses, some samples were analyzed between 3 and 5 times. Finally, in order to check the external reproducibility of the data, the Hg contents of a selection of samples were re-analyzed using the direct mercury analyzer RA-915 lab from LUMEX® at the University of Oxford, Department of Earth Sciences (Supplementary Table S3). The data obtained using these two methods are in good agreement for Hg contents ranging between 10 to 31420 ppb with a slope of 0.9 and MSWD = 3.4 (Supplementary Figure S1).

The concentrations of trace elements other than Hg were determined on the product glasses by Laser Ablation Inductively Coupled Mass Spectrometry (LA-ICPMS) analysis at the University of Oxford, Department of Earth Sciences. The instrument used was a Perkin-Elmer Nexion 300Q quadrupole mass spectrometer coupled to a New Wave Research 213 nm laser ablation system. The ablation spot diameter was 50 μm with the laser operating at 20 J/cm^2 and a repetition rate of 10Hz. Ablated material was transported to the Mass Spectrometer using He carrier gas. Four LA-ICPMS analyses were performed on each product glass (Supplementary Table S4) in addition to 4 analyses each of separate chips of the 2 glasses which had been combined to form the starting material (Table 1). Time resolved spectra were collected for each sample using SRM NIST 610 glass (Jochum et al., 2011) as the primary standard and the Ca content of the product glass, measured by electron microprobe, as the internal standard. GRE-1G glass (Jochum et al., 2005, Jochum et al., 2011) was used as a secondary standard to check the calibration. Data were reduced using Glitter (http://www.glitter-gemoc.com/) software. Some samples required all the glass for Hg content analysis and no EPMA and LA-ICPMS data could be collected (see supplementary Table S2).

One element, Tl was inadvertently omitted from the starting material analyses although approximately 50 ppm had been added to the basalt starting material. Our LA-ICPMS analyses of chips of the 2 glasses mixed to form the starting material (Table 1) indicate that both contain 55-65 ppm of Tl and therefore 60 ppm was used to calculate the partial pressure of Tl species during the experiment.

The oxidation states of a selection of the products (Supplementary Table S2) were determined from near edge structure at the Fe K-edge (XANES) on beamline I18 (microfocus spectroscopy) of the DIAMOND synchrotron. Spectra were collected in fluorescence mode using a Si 111 monochromator, a beamsize of 20 × 20 μm and with a 0.025-mm thick Al foil to attenuate the photon flux. Counts were collected for 1 second at each energy, with the energy

steps being as follows: 7050-7100 eV (5eV/step); 7100-7135 eV (0.2 eV/step); 7135-7180 eV(2 eV/step); 7180-7350 eV (5 eV/step). Spectra were normalized and fitted using Larch (Newville 2013). The pre-edge region between 7105 eV and ~7117 eV (normalized intensity of 0.2) was simultaneously fitted using Lorentzian and linear functions for the background, and two pseudo-Voigt peaks for the features corresponding to the 1s-3d transitions in Fe. To ensure fits were systematic and reproducible, peak linewidths (sigma) and centers were constrained to be within the same limits for all standards and samples. Standardizations were based on our measurements of the spectra of a series of Martian basalts (Matzen et al., 2022) which had their oxidation states determined by Mössbauer spectroscopy and for which the XANES spectra had been cross-calibrated against a series of basalt standards of known Fe^{3+}/Fe^{2+} loaned to us by Dr. E. Cottrell (Smithsonian Institution).

3. Results and discussion

3.1 Element loss as a function of time

Mercury was, as expected, lost very rapidly in the early stages of these sealed-tube experiments. As shown in Figure 2A-B, the initial content of ~93 ppm reduces to ~2.3 ppm after 5 min at 1300 °C. At this point the partial pressure of Hg species in the tube is calculated, to be approximately 0.0015 bar (150 Pa) (Supplementary Table S2) and it remains at this value throughout the remainder of the experiment. The partial pressure of Hg, (p(Hg)) in the gas phase was calculated from the ideal gas law by assuming that Hg^0 is monoatomic:

$$p(\mathrm{Hg})=mRT/V \quad [1]$$

In equation [1] m is the number of moles of Hg in the gas phase, R is the gas constant (8.3145 J. K^{-1}.mol^{-1}) T is the temperature (K) and V is the volume of the ampoule in m^3.

The Hg content of the melt declines further to <100 ppb after 10 min and remains stable at ~90-130 ppb after 6-24 hours. Other elements which are generally considered to be moderately volatile, notably Cd, Tl, In, Ag (Fig. 3A-B-C-D) Ga, Sn, Ge, Sb, Ga, Pb, Cs, Li (Table 2) behave in a similar fashion to Hg but with less extreme losses of the element from the melt. Experiments at 1400 °C (Fig. 2B) followed a similar pattern to those at 1300 °C (Fig. 2A), with rapid loss of almost all Hg and an apparent concentration plateau of 40 ppb after 1-3 hours.

For most elements the decline in concentration is not a simple function of time, but instead shows some scatter due, we believe, to several processes which are not readily quantifiable. One of these is infiltration into and reaction with the alumina crucible. For example, a thin layer of spinel is observed at the contact between the final glass and the alumina

crucible (more details in Supplementary Material A). This results from the reaction between the melt and the alumina crucible and modified the absolute Al_2O_3, FeO and MgO contents in the basaltic melt (Tables S1 and S5). By increasing the experiment duration and temperature, we observe a global increase of Al_2O_3 and a small decrease of MgO and FeO contents. For example, at 1300 °C, Al_2O_3 contents increase from 14.6 ± 0.1 to 22.8 ± 0.4 after 24 hours (Table S1) while MgO and FeO decrease by 2.0 and 1.6 wt.% respectively (see Supplementary Material A for more details).

The effect of spinel growth is most clearly seen in the behavior of the elements Ni and Co which are relatively involatile under these conditions of temperature and fO_2 (~1 logfO_2 unit below the FMQ buffer) but which nevertheless decline in concentration with time as shown in Figure 4A-B. The pattern of decline is less abrupt than in the cases of the more volatile elements however and resembles the pattern expected in the case of diffusion out of a source of limited extent (Crank, 1975). Partitioning into the growing spinel layer is expected in the cases of Ni^{2+} and Co^{2+} because both elements have stable spinel-structured aluminates of general formula MAl_2O_4 and are observed to partition strongly from basaltic melt into spinel (Righter et al., 2006). Righter et al. (2006) obtained best fit values of D_{Ni} and D_{Co} (spinel/melt) of 10 and 5 respectively at 1150-1250ºC and oxygen fugacities close to FMQ. These values confirm our hypothesis that these 2 elements were lost from melt to the growing spinel layer. For Zn, the study of Neuman et al. (2022) reported Zn partition coefficients between spinel and basaltic melts ($D_{(Zn)\ spinel/melt}$) ranging from 3 to 40 with an average of 5 ± 2. It seems probable, therefore that a significant fraction of Zn was also lost to the spinel layer. The situation with Cu is less clear because Cu^{2+} also forms a stable aluminate, but we would expect Cu to be in the 1+ oxidation state under the relatively reducing conditions of the experiments. To confirm this we calculated the log(Cu^{2+}/Cu^{+}) ratio for representative samples using the Miller et al. (2024) equation and obtained a $Cu^{+}/\Sigma Cu$ ~0.99. Nevertheless, both Zn and Cu exhibit similar behavior to Ni and Co (Fig. 5A-B) suggesting that some of the loss of both these 2 elements is due to reaction with the crucible (i.e., due to spinel formation - Supplementary Material A) rather than escape to the atmosphere in the ampoule.

3.2 Fractional loss, speciation in the gas phase and comparisons with other measures of volatility

We calculated the fraction of loss of each element from the melt, using the assumption that all loss of nominally volatile elements was to the ampoule atmosphere, even that of Zn and Cu. In the latter cases the calculated masses lost to the atmosphere are maximum possible values. The

input data and results from our calculations are presented in Table 2. Comparison with earlier studies of element volatility (e.g., Norris and Wood, 2017; Sossi et al., 2019; Ni et al., 2021; Zhang et al., 2021; Neuman et al., 2022; Califano et al., 2025) is interesting and informative. We should note, however, that all earlier studies were performed in open systems where the volatile elements are completely lost during the experiment, whereas our data refer to closed-system volatilities where the elements are all retained in the gas phase in contact with the melt. In the case of open-system experiments factors such as element evaporation coefficients and flow velocities of the gas phase are potentially important influences on results. These effects are absent in our experiments. Bearing in mind these potential influences on data in the literature, we compared the volatilities obtained in our study with previous experimental results obtained under conditions similar or close to ours. Specifically, we compared our data at 1300 °C for 60 minutes (Table S4) with studies performed in open systems (one-atmosphere gas mixing furnaces) at comparable temperatures, oxygen fugacities and durations, notably those by Norris and Wood (2017), Sossi et al. (2019) and Califano et al. (2025). As starting material, Norris and Wood (2017) used a natural Icelandic basalt, Sossi et al. (2019) a planetary mantle-like composition and Califano et al. (2025) used a natural shoshonitic basalt. We compared the ratio (X_t/X_0) corresponding to the elemental retention in the glass phase after fixed experiment time (X_t) normalized to the initial contents (X_0). The resulting values are compared in Figure 6 (for experiments at 1300 °C and 60 minutes) and are focused on elements common to the different studies, including Ag, Cd, Cr, Cu, Ga, Ge, Li, Rb, V, and Zn. As can be seen in Figure 6, there is decreasing retention of an element in the melt as we progress from Li (least volatile) to Cd (most volatile). This general trend is observed in all 4 studies although in detail there are considerable differences due to the ways in which particular experiments were conducted.

Our results exhibit generally good agreement (within 30 %) with those of Califano et al. (2025) for Cu, Zn, Ga, Ag, and Cd. Small discrepancies can be attributed to differences in redox conditions, i.e., ~FMQ –1 in our experiments versus FMQ +1.7 in Califano et al. (2025). Another parameter that can explain some differences is the Cl activity (a_{Cl}). Since Califano et al. (2025) added 1 wt. % NaCl to their starting material, the a_{Cl} during their experiments was significantly higher than in ours and should increase volatilities of elements such as alkalis, silver and copper. Agreement with the data of Norris and Wood (2017) is also quite good except for Ge. The enhanced loss of this element from the Norris and Wood (2017) experiments is possibly due to dissolution in the Ni crucible which they used. The most challenging comparison in terms of differences in experimental setup is that with the data of Sossi et al.

(2019) who measured evaporation from small beads (25 mg) of melt with large surface area/volume ratio and thus with rapid volatile loss. For this reason, despite reasonably good agreement of their data with ours for Li, Cr and Ga, they observe much larger losses of the volatile elements Cu, Zn, Ge, Rb, Ag and Cd in 60 minutes than we do.

Figure 6 shows the comparison of our volatility results in a closed system with open-system data from the literature. Better comparisons would be with closed system data from the literature, but the only general closed-system results are those relating to condensation in the solar nebula. In this case the gas and condensd phases remain in equilibrium with one another, as in our experiments, during cooling at very low oxygen fugacity. Figure 7 is a plot of fraction lost of the most volatile elements plotted against the temperature at which 50 % of the element would have condensed in the solar nebula (Wood et al., 2019). There are, of course, significant differences in the conditions of the two processes. We are studying volatility from a silicate melt at an oxygen fugacity about 1 logfO_2 unit below the FMQ buffer whereas the condensation calculation addresses precipitation into a range of solid metals, silicates and sulfides at an oxygen fugacity approximately 10 logfO_2 units below the FMQ buffer. Nevertheless there is a reasonable correlation between these 2 measures of volatility based on evaporation from melt and condensation to solid (Fig. 7). This broad agreement led us to consider whether speciation in the gas phase might be similar in the two cases.

Wood et al. (2019) provide information and data sources for speciation calculations during condensation in the solar nebula. Alkali elements are predominantly speciated as MCl^0 in the gas phase at their condensation temperatures whereas most of the other elements of concern in Figure 7 are present as M^0, MS^0 or MCl^0 species depending on the abundance and condensation temperature of chlorine. Here we used HSC Chemistry software and databases (https://www.metso.com/portfolio/hsc-chemistry/) to calculate speciation in the atmosphere inside the ampoules. The GEM module in HSC chemistry performs equilibrium calculations by free energy minimization under specified conditions of composition, temperature, pressure and oxygen fugacity. It is widely used in equilibrium speciation calculations for volcanic gases and its application has been extensively discussed in the literature (Symonds and Reed, 1993; Gerlach, 2004; Martin et al, 2006). Given the presence of virtually all of the F (480 ppm) and Cl (590 ppm) in the atmosphere, we find that alkali elements are complexed largely with F and Cl as LiF^0, $CsCl^0$, CsF^0, $NaCl^0$, NaF^0, RbF^0 (Table 3). Gaseous oxides dominate for other elements, namely TlO, GeO, Ga_2O, In_2O, SnO and AsO, while uncharged M^0 species are major contributors to gaseous Hg, Cd, Zn, Cu, Pb, Ag, Sb and Rb. It appears, therefore that there are

strong similarities between the dominant gaseous species in the case of condensation in the solar nebula and evaporation from silicate melts at 1300 °C (Table 3) despite the differences in oxygen fugacity and in the nature of the condensed phases.

The most significant outliers off the broad correlation between the fraction remaining in the melt in our experiments and the 50 % condensation temperatures are Pb and Sn (less volatile in the evaporation from silicate melt experiments than the solar nebula calculations) and Li and As (more volatile in our experiments than the solar nebula calculations). For Pb and Sn the difference could be due to the formation of more volatile sulfide species in the gas under solar nebula conditions, with such species being unstable in our experiments. In the cases of Li and As, Li forms LiF and As forms AsO under our experimental conditions and these species are absent in the nebula scenario, rendering Li and As less volatile. We should note, however, that stable species differences are also true for other elements without displacing them from the volatility trend. Specifically, given the significant differences in fO_2 conditions between our evaporation experiments and solar nebula calculations we might expect elements that preferentially stabilize as gas-phase oxides to be more volatile in the experiments. While this is the case for As, however, In and Ga do not show this relationship, possibly due to the involvement of halides as alternative stable species under oxidizing conditions.

3.3 Comparison with volcanic emission

In order to relate our results to volcanic emissions on the present-day Earth, we compared the metal gas-phase speciation obtained at 1150 °C (Table 3) – taken as closest to magmatic temperatures – from HSC chemistry for our experiments with that derived from measurements of the gases being released at Etna (Aiuppa et al., 2008; Pyle and Mather 2009; Schiavi et al., 2006, Gennaro et al., 2019) and at Masaya (Martin et al., 2010; Moune et al., 2010; Mather et al., 2006). In both cases H_2O dominates, comprising 67 % (by mass) of emitted gas at Etna and 86.5 % at Masaya. CO_2 makes up 21 and 6.7 % at Etna and Masaya respectively while SO_2 (8.4 and 5 %), HCl (2.7 and 1.66 %) and HF (0.4 and 0.18 %) are significant minor species.

These compositions were used in conjunction with the same speciation software (HSC chemistry) at 1 bar pressure and 1150 °C to calculate the expected major species of each element being emitted. Results, presented in Table 3, again show that speciation in the 2 volcanic systems considered is very similar to that in our experiments, notably for the most volatile elements Hg, Tl and Cd. Figure 8 shows a comparison between the observed fraction of each element remaining in the melt at 1300 °C and the mean volatility coefficient calculated from

the element loss behavior observed from field measurement of emissions from Etna and Masaya's magmas when corrected for silicate fragments (Mather, 2015). As can be seen in Figure 8, there is a broadly good correlation between the experimental measurements of volatility and observations in natural systems. This correlation is very good in cases where the speciation is the same or similar in both cases, ie., for the elements Hg, Tl, Cd, and Ge. Outliers can generally be explained by differences in gas speciation. This is the case for Sb, which is more volatile in the natural examples because of the high HCl contents of the gases emitted and the stability of gaseous SbCl. This species is not calculated to be significant in the experimental environment. Similarly Pb appears to be less volatile in the experiments than in nature because of the low Cl content of the experimental gas. In contrast, Li is more volatile in the experiments, possibly due to the relatively high F content of the ampoule gas and the high stability of gaseous LiF.

Arsenic, for which AsO is the dominant gas species in both experimental and natural environments is apparently more volatile in nature than would be expected based on the experiments. This is an example of the effect of oxygen fugacity on speciation. The oxygen fugacity in our experiments was approximately 1 logfO_2 unit below the FMQ buffer (FMQ -1) (Supplementary Table S2) while oxygen fugacity at Etna and Masaya is estimated to be 2-3 logfO_2 units higher (Mather et al, 2006; Gennaro et al. 2019). Raising oxygen fugacity stabilizes gaseous oxide species such as AsO, leading to slightly enhanced volatility in nature as compared to our experiments. Other elements such as Cu, Ag, Zn, Cs, Sn and In lie close to the experiment-nature correlation despite having differences in their gaseous speciation. We note, however, that for these elements the most important species occurring in the experiments also tends to be one of the major species in nature which therefore explains the observed broad agreement in volatilities.

In summary, we find that the volatilities determined in our experiments are generally a good model for measured magmatic metal degassing from basalts like Masaya and Etna and calculated values for condensation from the solar nebula. This applies particularly to the very volatile elements Hg, Tl and Cd. The important new data generated here enable calculation of the equilibrium partial pressures of elemental species above natural basaltic melts and by extension the activities of the metal components in the melts themselves. Such data can be applied, for example, to degassing processes on asteroidal and planetary bodies in addition to volatile losses during terrestrial volcanism.

4. Conclusions

Characterizing metal volatility from silicate melts is of broad geochemical importance in terms of understanding trace metal behavior during planet formation, ore-deposition and the volcanic emissions of metals. In order to develop such understanding we undertook experiments to investigate the volatilities of Hg and other volatile trace metals. We find that Hg, as Hg^0 is almost instantaneously lost from silicate melts at 1 atm pressure, probably during heating to the solidus. In order to counteract this problem and allow study of the Hg degassing process we used the "sealed-tube" method of retaining Hg and other volatile elements in the atmosphere above molten silicate for periods of up to 24 hours at 1300 °C. Concentrations in the melt stabilize after <6 hours at 1300 °C (Figures 2 and 3) enabling us to calculate the equilibrium partial pressure of the species of an element of interest above a melt containing a known amount of that element. In this case we concentrated on Hg, but for comparative purposes added known amounts of Ag, As, Cd, Cr, Cs, Cu, Ga, Ge, In, Li, Pb, Rb, Sb, Sn, Tl, Zn, F and Cl to the starting basalt. Post-hoc analyses of the XANES spectrum of Fe in the quenched glasses revealed no change in oxidation state during the experiments, indicating that the oxygen fugacity remained about 1 logfO_2 unit below the buffer throughout (Supplementary Table S2).

The equilibrium partial pressure of Hg^0 above basaltic melts containing ~100 ppb Hg at 1300 °C and ~40 ppb Hg at 1400 °C was found to be about 150 Pa. This means that the Hg added to the starting material was >99 % degassed. Other volatile metals exhibit similar but less extreme volatility. Cd, for example, degasses 78 % of its inventory to 714 Pa of gaseous species in equilibrium with melt containing 71 ppm of the element (Table 2) while 77 Pa of Tl species (80 % degassed) are in equilibrium with 12 ppm of the element in the melt. The relative volatilities of the trace elements added to the melt follow the order Hg>>Tl>Cd>In>Zn*>Li>Cs>Cu*>As>Ag>Pb~Sn~Ga>Ge~Sb (asterisked elements uncertain and maximum possible volatilities adopted) and are quantified in terms of melt concentration, gas partial pressure and fraction lost from melt to gas in Table 2. We found that F and Cl were almost completely vaporized from the melt into the gas phase where they formed stable gaseous halides with a number of volatile metals notably the alkalis. At oxygen fugacity close to FMQ, oxide gas species dominate for Tl, Ge, Ga, As, In and Sn while uncharged M^0 species are major contributors to gaseous Hg, Cd, Zn, Cu, Pb, Ag, Sb and Rb in the experiments.

In order to place our results into context we compared volatilities in our experiments with volatilities from open-system experiments. We found relatively good agreement with the Califano et al. (2025) and Norris and Wood (2017) volatilities obtained from 60 minute experiments at 1300 °C. We observed greater differences with the results of Sossi et al. (2019), but these differences are explicable by the higher surface area/volume ratio used in their study,

a factor that enhances volatile loss. We then compared our results with volatilities in two dramatically different environments. The first of these is the solar nebula, in which pressures were low (~10^{-4} bar) and elements condensed from H-rich gas into solid phases including Fe-rich metal, FeS, olivine and feldspar (Wood et al., 2019). Despite the large differences in oxygen fugacity (9 logfO_2 units) and in the nature of the condensed phases, silicate melt versus crystalline, there is a broadly good correlation between volatilities in our experiments and the condensation temperatures of the elements of interest from the solar nebula (Fig. 7). This agreement derives principally from similarities in the compositions of the gaseous species in equilibrium with the condensed phases and the fact that both condensation calculations and our experiments are closed-systems with continuous re-equilibration of gas and condensed phases. Gas species in these 2 cases are dominated by uncharged M^o species and halides MF and MCl. A second, comparison for our data is with measured volatilities during terrestrial volcanic degassing. We compared our volatility estimates with those calculated by Mather (2015) from gases/particles collected at Etna and Masaya volcanoes and lava concentrations (Fig. 8). In these cases the gases being emitted are rich in H_2O and contain significant amounts of HCl and HF in addition to CO_2 and SO_2. Speciation calculations for the trace gaseous metals at these locations indicate that chloride species are significant for a number of metals (Cu, In, Pb, Sn, Ga, Sb, Zn) in addition to the alkalis (Table 3). Nevertheless, the species which dominate in our experimental charges are also significant in abundance for most of these elements in the natural conditions also. The consequence of this observation is that there is a good correlation between the volatilities measured in our experiments and those measured in nature. The principal elemental exceptions are Sb and Pb which are less volatile in the experiments than in the natural systems and Li which is less volatile in natural volcanic systems. These differences can be explained in terms of differences in the stable gas species between the experiments and the halogen-rich volcanic emissions. Most importantly however, Hg has the same major gaseous species, Hg^o in all environments investigated. The same applies to the next two most volatile elements, the best comparators to Hg, the metals Tl and Cd. We conclude that, with one or two exceptions our experiments are a good model for metal volatilities in nature and that the major element composition of the gas, particularly its halogen and sulfur contents play an important role.

In summary our experimental data confirm and emphasize the extremely volatile nature of Hg. Hg was by far the most volatile of the elements studied in our experiments, being >99 % degassed in a few minutes at 1300 °C. This compares with 80 % degassing of Tl and 78 %

degassing of Cd. Our data are the first measurements of the partial pressures of trace volatile metals in equilibrium with known concentrations of the elements in the melt. Importantly, the data were obtained at known fugacity of oxygen, and approximately known concentrations of Cl and F in the gas phase. They therefore represent a starting point for quantitative calculations of volatility and volatile loss in volcanic and magmatic systems.

5. Acknowledgements

We acknowledge with thanks the help of Laurent Tissandier (Nancy) in the establishment of the experimental method and Andrew Matzen (Oxford) who provided us with the fused basaltic starting material. We thank the SARM service from CRPG (Nancy) and Joost Frieling (Oxford) for their contributions for the final run products characterizations. We also thank the three reviewers, an anonymous reviewer, Hanna Nekvasil and Paolo Sossi for their constructive comments and suggestions helping to improve this manuscript. Mary Ayyamperumal and Sonja Aulbach are gratefully thanked for their editorial handling and comments. The research was funded by the European Research Council Consolidator Grant V-ECHO (ERC-2018-COG-8187 17-V-ECHO).

Figure captions

Figure 1. Picture of an experimental ampoule which had been run (experiment FM 252) at 1300 °C for 30 minutes before quenching in air.

Figure 2: Hg content as a function of time and experiment duration for two temperatures 1300 °C (A) and 1400 °C (B). Curves are only guides for the eyes to show Hg content decreasing from the initial Hg content (i.e., 93000 ppb)

Figure 3: (A), (B), (C) and (D) show decline in concentration with time for Tl, Cd, In and Ag respectively, at 1300 °C. Note similar form to the decline observed for Hg, but lesser extents of total loss.

Figure 4. A and B shows the decline in concentration of the involatile elements Ni and Co respectively, in our experiments at 1300 °C. We believe that this is due to infiltration into and reaction with the alumina crucible.

Figure 5. Concentrations of (A) Cu and (B) Zn, expected to be volatile, as a function of time and at 1300 °C.

Figure 6. Comparison of volatilities, determined as fraction of element remaining X_t (Table S4) divided by initial concentration X_0 from this study (Table 1) with literature data obtained under similar conditions of temperature (1300 °C), time (60 minutes) and for fO_2 ranging from FMQ -1.0 to FMQ +1.7.

Figure 7. Plot of fraction remaining in the melt at 1300 °C after 6-24 hours (plateau region in Figs. 2-5) versus the temperature at which the element of interest would be 50 % condensed into solids in the solar nebula at 10^{-4} bar (Wood et al., 2019).

Figure 8. The fraction remaining at 1300 °C in the melt after 6-24 hours (plateau region in Figs. 2-5) plotted against the Mean Volatility Coefficient (Mather 2015) estimated from measurements at Etna and Masaya.

References

Aiuppa A., Giudice G., Gurrieri S., Liuzzo M., Burton M., Caltabiano T., McGonigle A.J.S., Salerno G., Shinohara H., Valenza, M. (2008). Total volatile flux from Mount Etna. *Geophysical Research Letters*, *35*(24). https://doi.org/10.1029/2008GL035871

Bagnato E., Aiuppa A., Parello F., Calabrese S., D'alessandro W., Mather T.A., McGonigle A.J.S., Pyle D.M., Wängberg I. (2007). Degassing of gaseous (elemental and reactive) and particulate mercury from Mount Etna volcano (Southern Italy). *Atmospheric Environment*, *41*(35), 7377-7388. https://doi.org/10.1016/j.atmosenv.2007.05.060

Bagnato E., Barra M., Cardellini C., Chiodini G., Parello F., Sprovieri M. (2014). First combined flux chamber survey of mercury and CO2 emissions from soil diffuse degassing at Solfatara of Pozzuoli crater, Campi Flegrei (Italy): Mapping and quantification of gas release. *Journal of Volcanology and Geothermal Research*, *289*, 26-40. https://doi.org/10.1016/j.jvolgeores.2014.10.017

Berthelot, M. (1872). On the law which governs the distribution of a substance between two solvents. *Ann. Chim. Phys*, *26*(9).

Blundy J., Afanasyev A., Tattitch B., Sparks S., Melnik O., Utkin I., Rust A. (2021). The economic potential of metalliferous sub-volcanic brines. *Royal Society Open Science*, *8*(6), 202192. https://doi.org/10.1098/rsos.202192

Boulliung J., Wood B. J. (2022). SO2 solubility and degassing behavior in silicate melts. *Geochimica et Cosmochimica Acta*, *336*, 150-164. https://doi.org/10.1016/j.gca.2022.08.032

Boulliung J., Wood B.J. (2023). Sulfur oxidation state and solubility in silicate melts. *Contributions to Mineralogy and Petrology*, *178*(8), 56. https://doi.org/10.1007/s00410-023-02033-9

Califano E., Mollo S., Sossi P.A., Tavazzani L., Moschini P., Pontesilli A., Scarlato P. (2025). Volatilities and diffusivities of Tl, Ag, Cu, Pb, Cd, Zn, Ga, and As from a Cl-bearing shoshonitic basalt and their application to volcanic degassing. *Chemical Geology*, 122947. https://doi.org/10.1016/j.chemgeo.2025.122947

Carignan J., Hild P., Mevelle G., Morel J., Yeghicheyan D. (2001). Routine analyses of trace elements in geological samples using flow injection and low pressure on-line liquid chromatography coupled to ICP-MS: A study of geochemical reference

materials BR, DR-N, UB-N, AN-G and GH. *Geostandards Newsletter*, *25*(2-3), 187-198. https://doi.org/10.1111/j.1751-908X.2001.tb00595.x

Crank J. (1975). The Mathematics of Diffusion. Second edition. Oxford University Press.

Cooke D. R., Hollings P., Wilkinson J. J., Tosdal R. M., Turekian H. D. H. K. (2014). 13.14—Geochemistry of porphyry deposits. *Treatise on geochemistry*, *13*, 357-381. https://doi.org/10.1016/B978-0-08-095975-7.01116-5

Driscoll C. T., Mason R. P., Chan H. M., Jacob D. J., Pirrone N. (2013). Mercury as a global pollutant: sources, pathways, and effects. *Environmental science & technology*, *47*(10), 4967-4983. https://doi.org/10.1021/es305071v

Fendley I. M., Frieling J., Mather T. A., Ruhl M., Hesselbo S. P., Jenkyns H. C. (2024). Early Jurassic large igneous province carbon emissions constrained by sedimentary mercury. *Nature Geoscience*, *17*(3), 241-248. https://doi.org/10.1038/s41561-024-01378-5

Foucaud Y., Fabre C., Demeusy B., Filippova I.V., Filippov L.O. (2019). Optimisation of fast quantification of fluorine content using handheld laser induced breakdown spectroscopy. *Spectrochimica Acta Part B: Atomic Spectroscopy*, *158*, 105628. https://doi.org/10.1016/j.sab.2019.05.017

Gennaro M.E., Paonita A., Iacono-Marziano G., Pichavant M., Liotta M., Rizzo A. L., Martel C., Rotolo S.G. (2019). Chemical and redox variations affected by differentiation in Mt. Etna (Italy) magmatic system. In *Geophysical Research Abstracts* (Vol. 21). https://hal.science/hal-03554263

Gerlach T.M. (2004). Volcanic sources of tropospheric ozone-depleting trace gases. *Geochemistry, Geophysics, Geosystems*, *5*(9). https://doi.org/10.1029/2004GC000747

Hedenquist, J. W., & Lowenstern, J. B. (1994). The role of magmas in the formation of hydrothermal ore deposits. *Nature*, *370*(6490), 519-527. https://doi.org/10.1038/370519a0

Hinkley T., Matsumoto A. (2007). Mid-Holocene change in types of degassing volcanoes, using indium in Antarctic ice as a tracer of volcanic source type. *Geophysical research letters*, *34*(17). https://doi.org/10.1029/2007GL030056

Hinkley T.K., Le Cloarec M.F., Lambert G. (1994). Fractionation of families of major, minor, and trace metals across the melt-vapor interface in volcanic exhalations.

Geochimica et Cosmochimica Acta, *58*(15), 3255-3263. https://doi.org/10.1016/0016-7037(94)90053-1

Jochum K.P., Nohl U., Herwig K., Lammel E., Stoll B., Hofmann A.W. (2005). GeoReM: a new geochemical database for reference materials and isotopic standards. *Geostandards and Geoanalytical Research*, *29*(3), 333-338. https://doi.org/10.1111/j.1751-908X.2005.tb00904.x

Jochum K.P., Weis U., Stoll B., Kuzmin D., Yang Q., Raczek I., Jacob D.E., Stracke A., Birdbaum K., Frick D. A., Günther D., Enzweiler J. (2011). Determination of reference values for NIST SRM 610–617 glasses following ISO guidelines. *Geostandards and Geoanalytical Research*, *35*(4), 397-429. https://doi.org/10.1111/j.1751-908X.2011.00120.x

Kellerhals T., Tobler L., Brütsch S., Sigl M., Wacker L., Gäggeler H.W., Schwikowski M. (2010). Thallium as a tracer for preindustrial volcanic eruptions in an ice core record from Illimani, Bolivia. *Environmental science & technology*, *44*(3), 888-893.

Kress, V.C., Carmichael, I.S.E., (1991). The compressibility of silicate liquids containing Fe2O3 and the effect of composition, temperature, oxygen fugacity and pressure on their redox states. Contributions to Mineralogy and Petrology 108(1-2), 82-92. doi.org/10.1007/bf00307328.

Lodders, K. (2003). Solar system abundances and condensation temperatures of the elements. *The Astrophysical Journal*, *591*(2), 1220.

Marie B., Marin L., Martin P. Y., Gulon T., Carignan J., Cloquet, C. (2015). Determination of mercury in one hundred and sixteen geological and environmental reference materials using a direct mercury analyser. *Geostandards and Geoanalytical Research*, *39*(1), 71-86. https ://doi.org/10.1111/j.1751-908X.2013.00254.x

Martin R.S., Mather T.A., Pyle D. M. (2006). High-temperature mixtures of magmatic and atmospheric gases. *Geochemistry, Geophysics, Geosystems*, *7*(4). https://doi.org/10.1029/2005GC001186

Martin R.S., Sawyer G.M., Spampinato L., Salerno G.G., Ramirez C., Ilyinskaya E., Witt M. L. I., Mather T. A., Watson J. C., Phillips C., Oppenheimer C. (2010). A total volatile inventory for Masaya Volcano, Nicaragua. *Journal of Geophysical Research: Solid Earth*, *115*(B9). https://doi.org/10.1029/2010JB007480

Martin R. S., Watt S.F.L., Pyle D.M., Mather T.A., Matthews N.E., Georg R.B., Day J.A., Fairhead T., Witt M.L.I, Quayle, B. M. (2009). Environmental effects of ashfall in

Argentina from the 2008 Chaitén volcanic eruption. *Journal of Volcanology and Geothermal Research*, *184*(3-4), 462-472. https://doi.org/10.1016/j.jvolgeores.2009.04.010

Mather T.A. (2015). Volcanoes and the environment: Lessons for understanding Earth's past and future from studies of present-day volcanic emissions. *Journal of Volcanology and Geothermal Research*, *304*, 160-179. https://doi.org/10.1016/j.jvolgeores.2015.08.016

Mather T.A., Pyle D.M., Tsanev V.I., McGonigle A.J.S., Oppenheimer C., Allen, A.G. (2006). A reassessment of current volcanic emissions from the Central American arc with specific examples from Nicaragua. *Journal of volcanology and geothermal Research*, *149*(3-4), 297-311. https://doi.org/10.1016/j.jvolgeores.2005.07.021

Mathieu R. (2009). *Solubilité du sodium dans les silicates fondus* (Doctoral dissertation, Institut National Polytechnique de Lorraine).

Mathieu R., Khedim H., Libourel G., Podor R., Tissandier L., Deloule E., Faure F., Rapin C., Vilasi M. (2008). Control of alkali-metal oxide activity in molten silicates. *Journal of non-crystalline solids*, *354*(45-46), 5079-5083. https://doi.org/10.1016/j.jnoncrysol.2008.07.004

Matzen A.K., Woodland A., Beckett J. R., Wood B.J. (2022). Oxidation state of iron and Fe-Mg partitioning between olivine and basaltic martian melts. *American Mineralogist*, *107*(7), 1442-1452. https://doi.org/10.2138/am-2021-7682

McDonough W.F., Sun S.S. (1995). The composition of the Earth. *Chemical geology*, *120*(3-4), 223-253. https://doi.org/10.1016/0009-2541(94)00140-4

Miller L.A., Berry A.J., O'Neill H. S. C., Wykes J., Newville M., Lanzirotti T. (2024). The effect of composition, temperature and pressure on the oxidation state and coordination environment of copper in silicate melts. *Geochimica et Cosmochimica Acta*, *364*, 129-147. https://doi.org/10.1016/j.gca.2023.07.021

Moune S., Gauthier P.J., Delmelle P. (2010). Trace elements in the particulate phase of the plume of Masaya Volcano, Nicaragua. *Journal of Volcanology and Geothermal Research*, *193*(3-4), 232-244. https://doi.org/10.1016/j.jvolgeores.2010.04.004

Nernst, W. (1891). Distribution of a substance between two solvents and between solvent and vapor. *Z. phys. Chem*, *8*, 110-139.

Neuman M., Holzheid A., Lodders K., Fegley Jr.B., Jolliff B.L., Koefoed P., Chen H., Wang, K. (2022). High temperature evaporation and isotopic fractionation of K and Cu. *Geochimica et cosmochimica acta*, *316*, 1-20. https://doi.org/10.1016/j.gca.2021.09.035

Newville M. (2013). Larch: an analysis package for XAFS and related spectroscopies. In *Journal of Physics: Conference Series* (Vol. 430, No. 1, p. 012007). IOP Publishing. doi:10.1088/1742-6596/430/1/012007

Ni P., Macris C.A., Darling E.A., Shahar A. (2021). Evaporation-induced copper isotope fractionation: Insights from laser levitation experiments. *Geochimica et Cosmochimica Acta*, *298*, 131-148. https://doi.org/10.1016/j.gca.2021.02.007

Norris C.A., Wood B.J. (2017). Earth's volatile contents established by melting and vaporization. *Nature*, *549*(7673), 507-510. https://doi.org/10.1038/nature23645

Nriagu J.O. (1989). A global assessment of natural sources of atmospheric trace metals. *Nature*, *338*(6210), 47-49. https://doi.org/10.1038/338047a0

Palme H., O'Neill H.S.T.C. (2014). Cosmochemical estimates of mantle composition. In *The mantle and core* (pp. 1-39). Elsevier. 10.1016/B978-0-08-095975-7.00201-1

Percival L.M., Bergquist B.A., Mather T.A., Sanei H. (2021). Sedimentary mercury enrichments as a tracer of large igneous province volcanism. *Large igneous provinces: A driver of global environmental and biotic changes*, 247-262. https://doi.org/10.1002/9781119507444.ch11

Pokrovski G.S., Borisova A.Y., Bychkov A.Y. (2013). Speciation and transport of metals and metalloids in geological vapors. *Reviews in Mineralogy and Geochemistry*, *76*(1), 165-218. https ://doi.org/10.2138/rmg.2013.76.6

Pyle D.M., Mather, T.A. (2003). The importance of volcanic emissions for the global atmospheric mercury cycle. *Atmospheric Environment*, *37*(36), 5115-5124. https://doi.org/10.1016/j.atmosenv.2003.07.011

Pyle D.M., Mather T.A. (2009). Halogens in igneous processes and their fluxes to the atmosphere and oceans from volcanic activity: A review. *Chemical Geology*, *263*(1-4), 110-121. https://doi.org/10.1016/j.chemgeo.2008.11.013

Righter K., Leeman W.P., Hervig R.L. (2006) Partitioning of Ni, Co and V between spinel-structured oxides and silicate melts: Importance of spinel composition. *Chemical Geology* 227, 1-25. https://doi.org/10.1016/j.chemgeo.2005.05.011

Roy N.K., Bose S.S. (2008). Determination of Mercury in Thirty-three International Stream Sediment and Soil Reference Samples by Direct Mercury Analyser. *Geostandards and Geoanalytical Research*, *32*(3), 331-335. https://doi.org/10.1111/j.1751-908X.2008.00851.x

Sanei H., Grasby S.E., Beauchamp B. (2012). Latest Permian mercury anomalies. *Geology*, *40*(1), 63-66. https ://doi.org/10.1130/G32596.1

Schiavi F., Tiepolo M., Pompilio M., Vannucci R. (2006). Tracking magma dynamics by laser ablation (LA)-ICPMS trace element analysis of glass in volcanic ash: The 1995 activity of Mt. Etna. *Geophysical research letters*, *33*(5). https://doi.org/10.1029/2005GL024789

Sossi P.A., Klemme S., O'Neill H.S.C., Berndt J., Moynier F. (2019). Evaporation of moderately volatile elements from silicate melts: experiments and theory. *Geochimica et Cosmochimica Acta*, *260*, 204-231. https://doi.org/10.1016/j.gca.2019.06.021

Sossi P.A., Stotz I.L., Jacobson S.A., Morbidelli A., O'Neill H. S. C. (2022). Stochastic accretion of the Earth. *Nature astronomy*, *6*(8), 951-960. https://doi.org/10.1038/s41550-022-01702-2

Symonds R.B., Reed M.H. (1993) Calculation of multicomponent chemical equilibria in gas-solid-liquid systems: Calculation methods, thermochemical data, and applications to studies of high-temperature volcanic gases with examples from Mt. St. Helens. *Am. J. Sci. 293, 8.* https://doi.org/10.2475/ajs.293.8.758

Thomas R.W., Wood B. J. (2021). The chemical behaviour of chlorine in silicate melts. *Geochimica et Cosmochimica Acta*, *294*, 28-42. https://doi.org/10.1016/j.gca.2020.11.018

Tsuchiyama A., Nagahara H., Kushiro I. (1981). Volatilization of sodium from silicate melt spheres and its application to the formation of chondrules. *Geochimica et Cosmochimica Acta*, *45*(8), 1357-1367. https://doi.org/10.1016/0016-7037(81)90228-3

Vernet M., Marin L., Boulmier S., Lhomme J., Demange J.C. (1987). Dosage du fluor et du chlore dans les matériaux géologiques y compris les échantillons hyperalumineux. *Analusis*, *15*(9), 490-498.

Wang F., Outridge P.M., Feng X., Meng B., Heimbürger-Boavida L.E., Mason R.P. (2019). How closely do mercury trends in fish and other aquatic wildlife track those in

the atmosphere?–Implications for evaluating the effectiveness of the Minamata Convention. *Science of the Total Environment*, *674*, 58-70. https://doi.org/10.1016/j.scitotenv.2019.04.101

Williams-Jones A.E., Heinrich C.A. (2005). Vapor transport of metals and the formation of magmatic-hydrothermal ore deposits: 100th anniversary special paper. *Economic Geology*, *100*(7), 1287-1312. https://doi.org/10.3929/ethz-b-000034971

Wood B.J., Smythe D.J., Harrison T. (2019). The condensation temperatures of the elements: A reappraisal. *American Mineralogist*, *104*(6), 844-856. https://doi.org/10.2138/am-2019-6852CCBY

Wood B.J., Walter M.J., Wade J. (2006). Accretion of the Earth and segregation of its core. *Nature*, *441*(7095), 825-833. https://doi.org/10.1038/nature04763

Zelenski M., Simakin A., Taran Y., Kamenetsky V.S., Malik, N. (2021). Partitioning of elements between high-temperature, low-density aqueous fluid and silicate melt as derived from volcanic gas geochemistry. *Geochimica et Cosmochimica Acta*, *295*, 112-134. https://doi.org/10.1016/j.gca.2020.12.011

Zhang Z.J., Nie N.X., Mendybaev R.A., Liu M.C., Hu J.J., Hopp T., Alp E.E., Bullock E.S., McKeegan K.D., Dauphas, N. (2021). Loss and isotopic fractionation of alkali elements during diffusion-limited evaporation from molten silicate: Theory and experiments. *ACS Earth and Space Chemistry*, *5*(4), 755-784. https://doi.org/10.1021/acsearthspacechem.0c00263

The authors declare that they have no competing interests

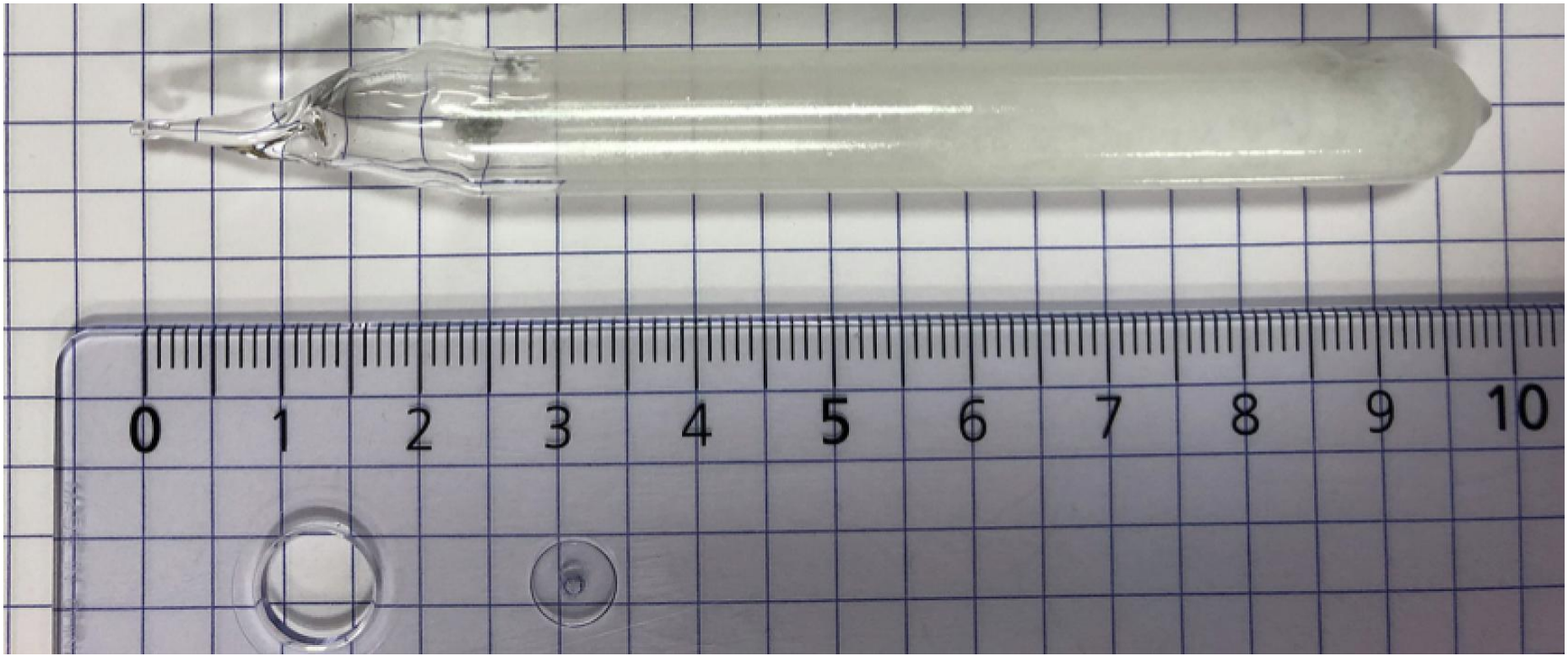

Figure 1

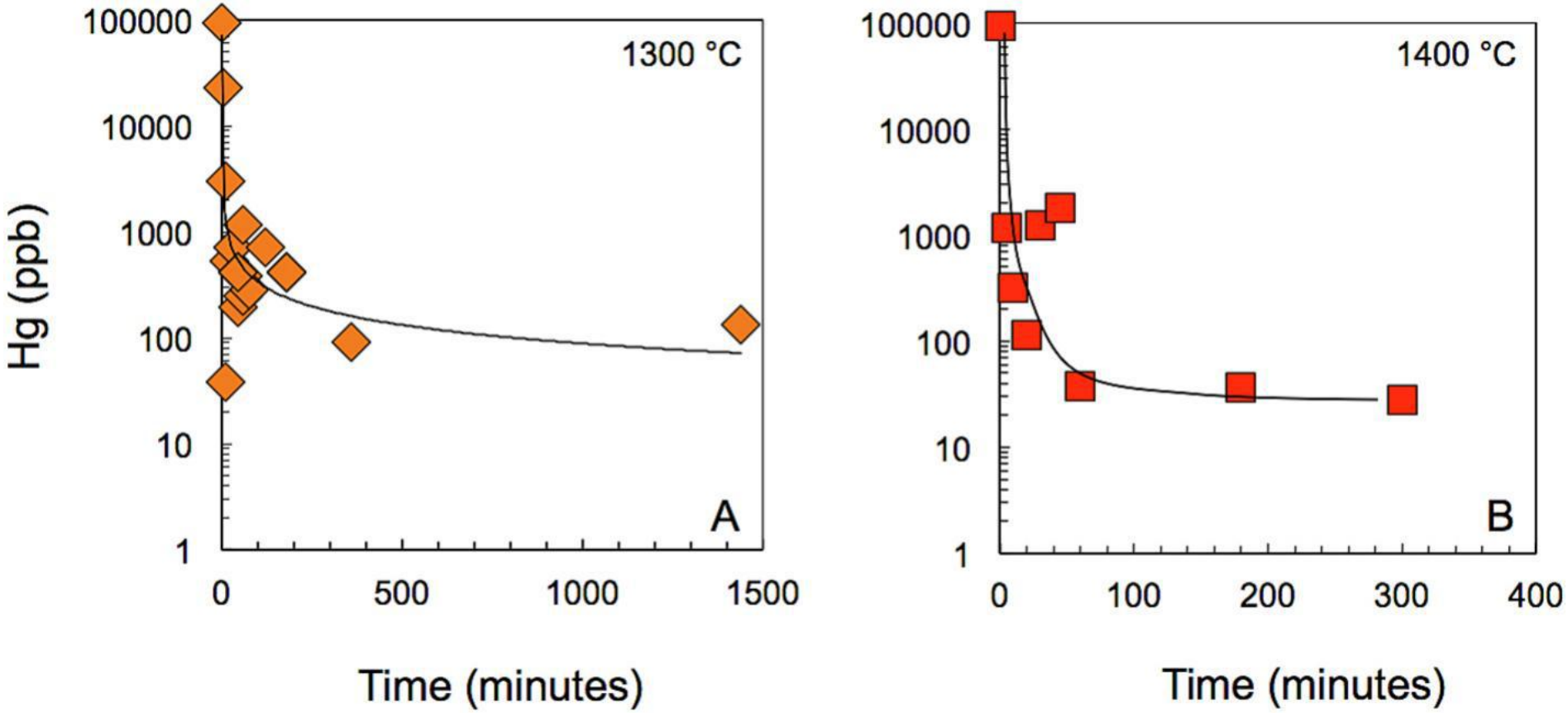
Hg (ppb)
100000
10000
1000
100
10
1
1300 °C
A
0
500
1000
1500
Time (minutes)
100000
10000
1000
100
10
1
1400 °C
B
0
100
200
300
400
Time (minutes)

Figure 2

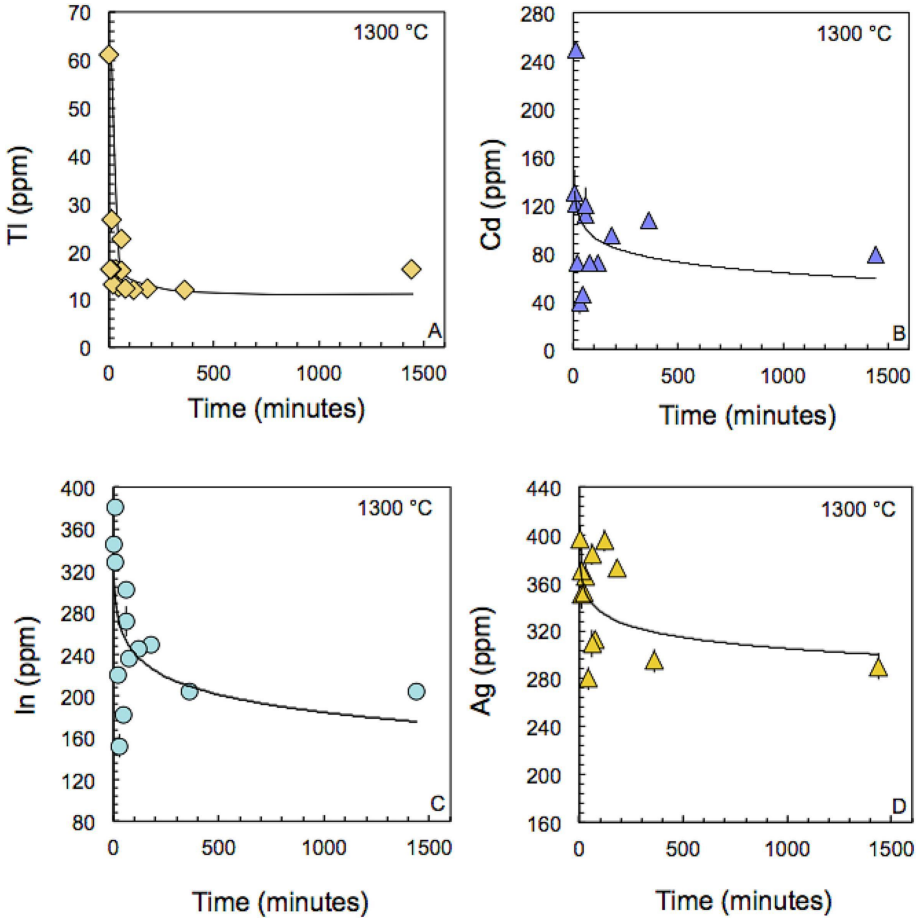
1300 °C
Tl (ppm)
Time (minutes)
A
1300 °C
Cd (ppm)
Time (minutes)
B
1300 °C
In (ppm)
Time (minutes)
C
1300 °C
Ag (ppm)
Time (minutes)
D

Figure 3

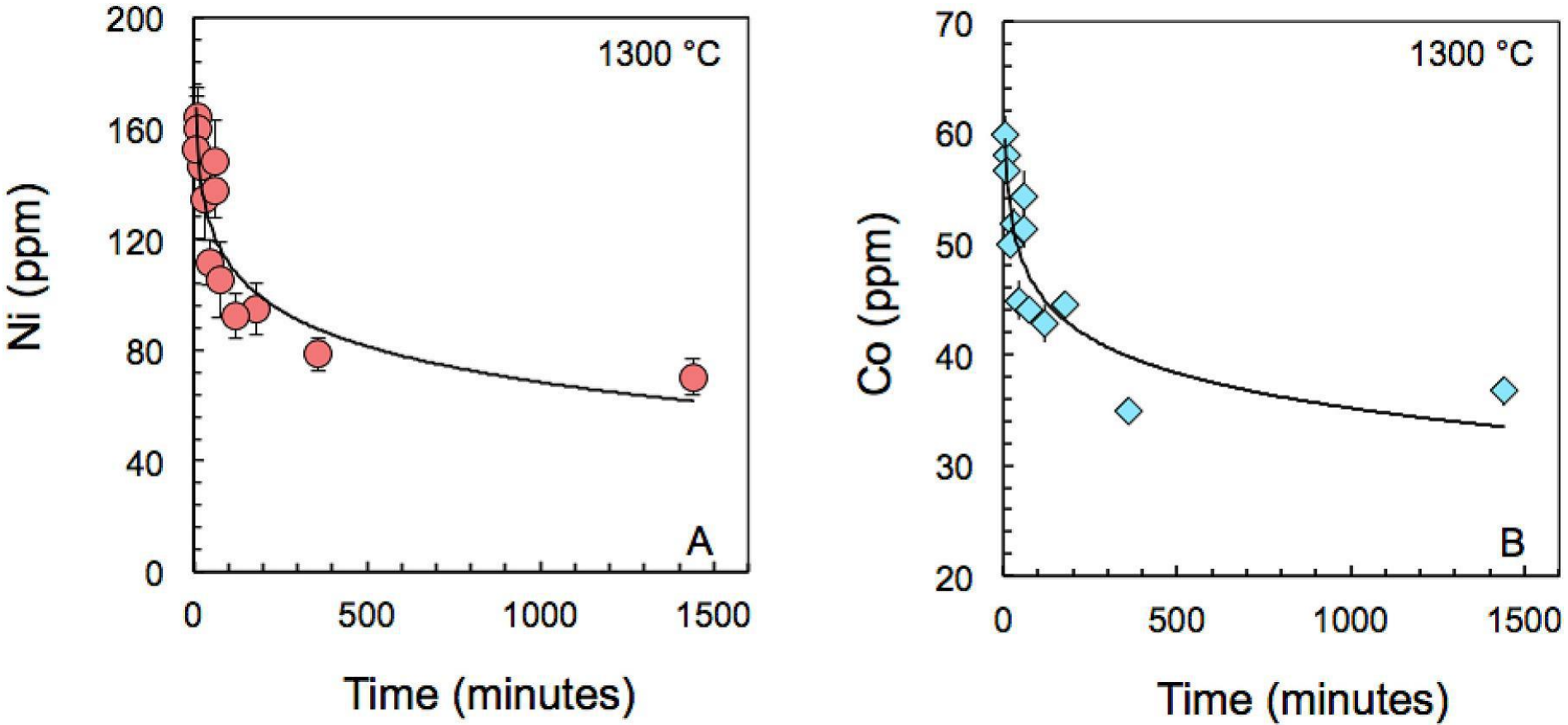
1300 °C
Ni (ppm)
200
160
120
80
40
0
0
500
1000
1500
Time (minutes)
A
1300 °C
Co (ppm)
70
60
50
40
30
20
0
500
1000
1500
Time (minutes)
B

Figure 4

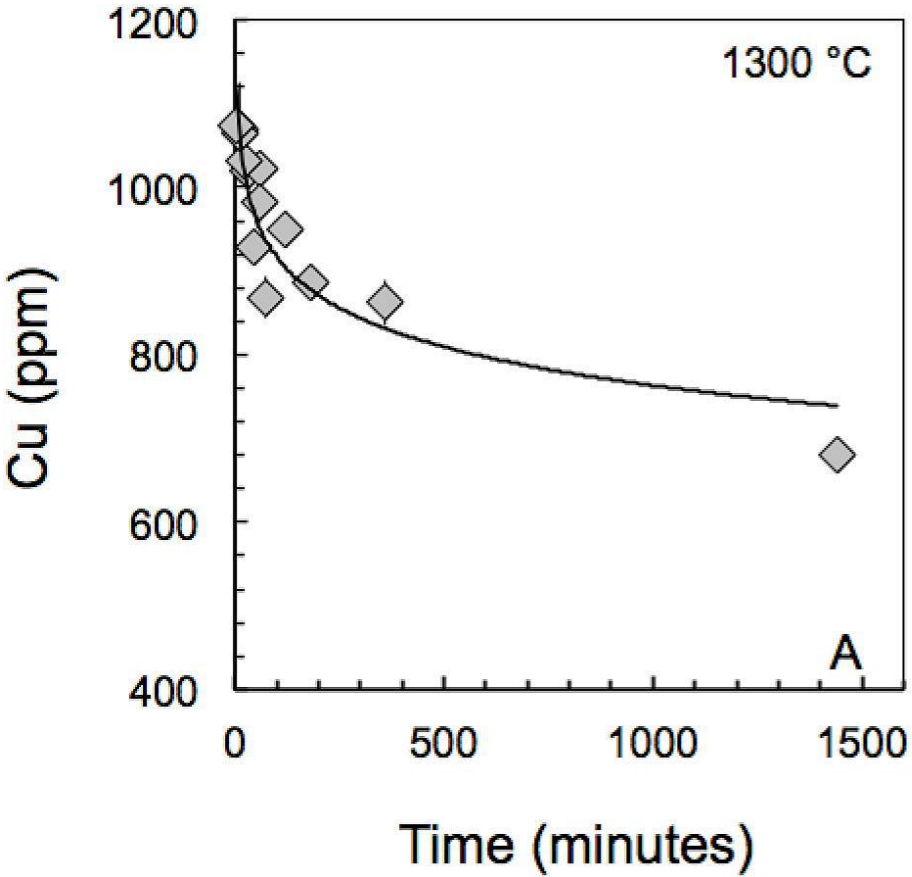
1300 °C
A
Cu (ppm)
1200
1000
800
600
400
0
500
1000
1500
Time (minutes)

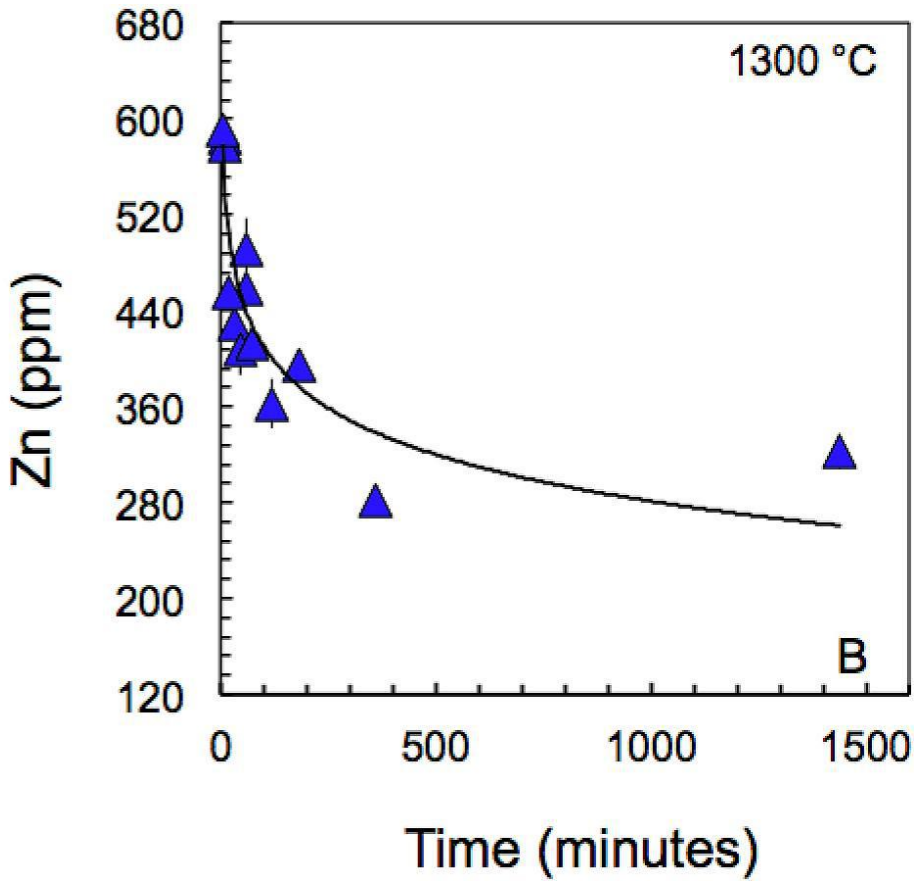
1300 °C
B
Zn (ppm)
680
600
520
440
360
280
200
120
0
500
1000
1500
Time (minutes)

Figure 5

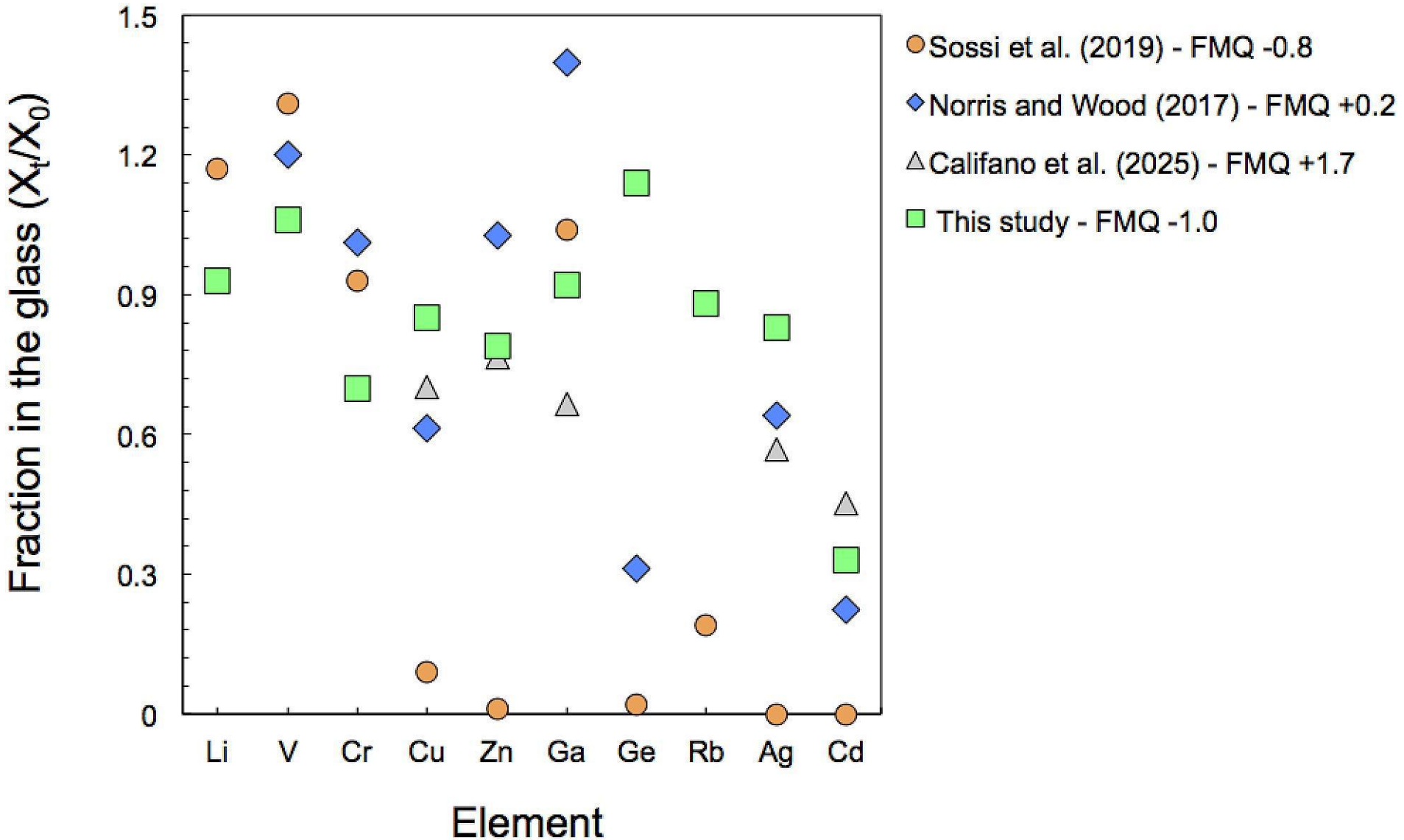
Fraction in the glass (X_t/X_0)
1.5
1.2
0.9
0.6
0.3
0
Li
V
Cr
Cu
Zn
Ga
Ge
Rb
Ag
Cd
Element
Sossi et al. (2019) - FMQ -0.8
Norris and Wood (2017) - FMQ +0.2
Califano et al. (2025) - FMQ +1.7
This study - FMQ -1.0

Figure 6

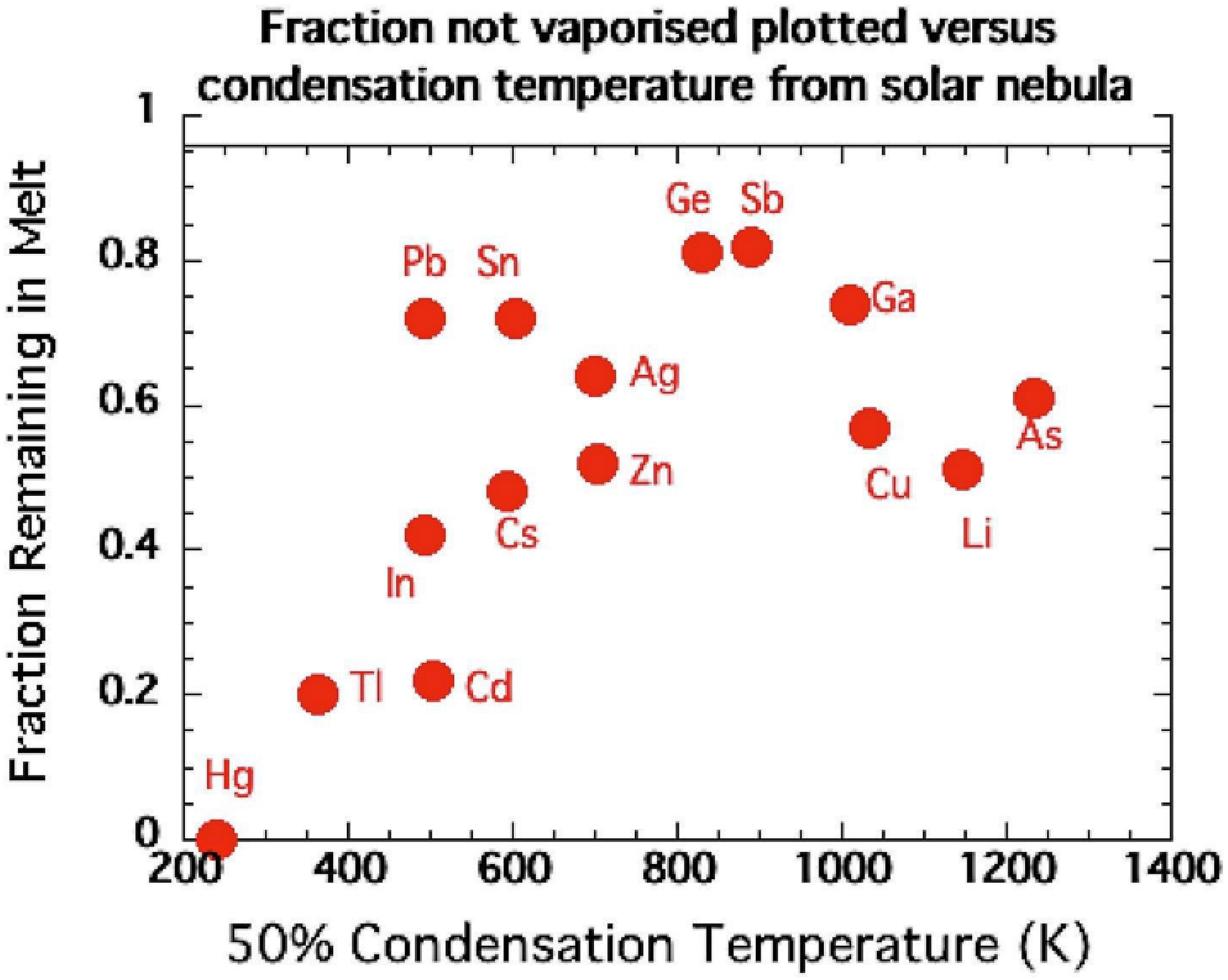
Fraction not vaporised plotted versus
condensation temperature from solar nebula
Fraction Remaining in Melt
1
0.8
0.6
0.4
0.2
0
200
400
600
800
1000
1200
1400
50% Condensation Temperature (K)
Ge
Sb
Pb
Sn
Ga
Ag
As
Zn
Cu
Cs
Li
In
Tl
Cd
Hg

Figure 7

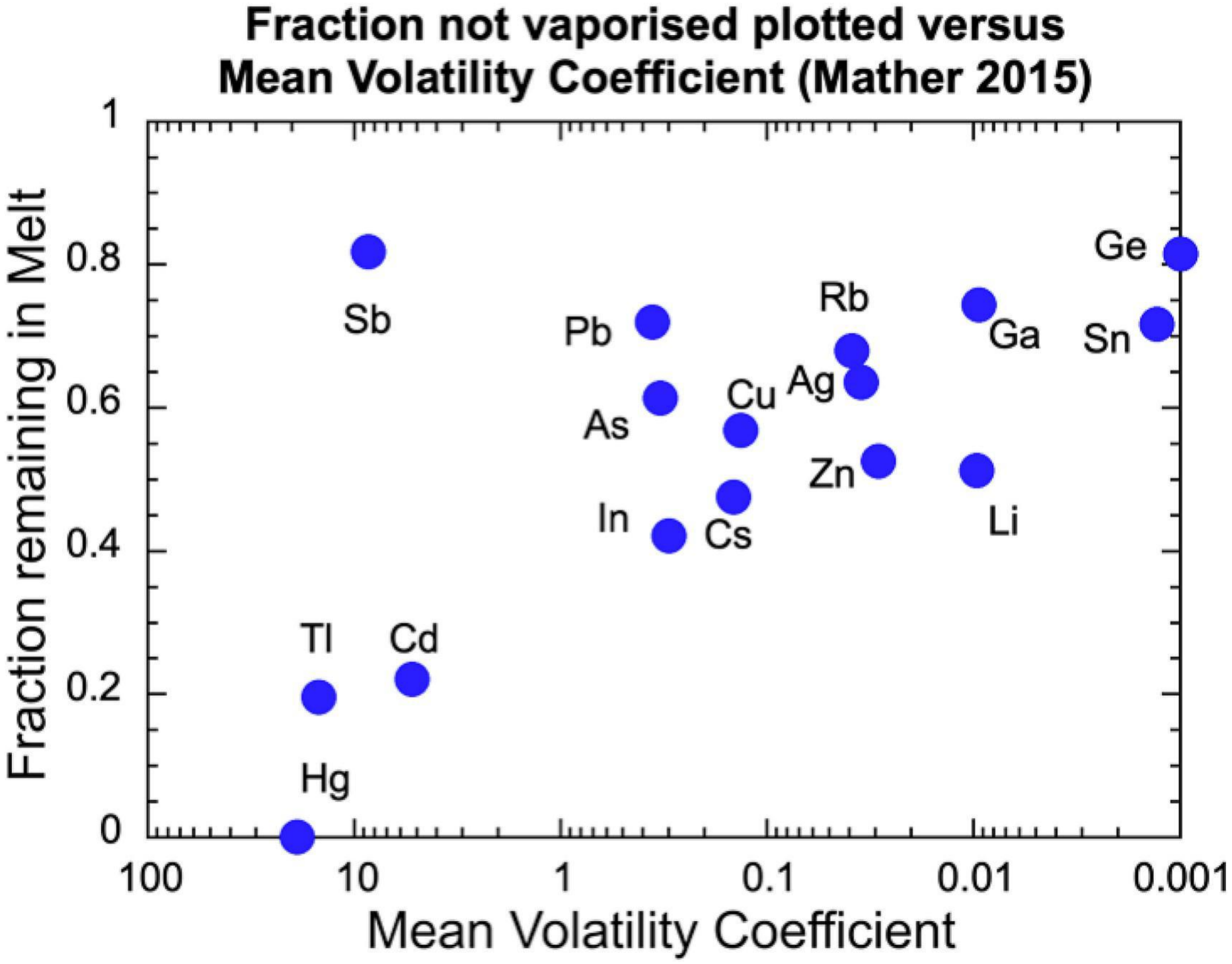
Fraction not vaporised plotted versus
Mean Volatility Coefficient (Mather 2015)
Fraction remaining in Melt
1
0.8
0.6
0.4
0.2
0
Sb
Pb
Rb
Ga
Ge
Sn
Ag
Cu
As
Zn
Li
In
Cs
Tl
Cd
Hg
100
10
1
0.1
0.01
0.001
Mean Volatility Coefficient

Figure 8